Design and Optimization of Support Structures for Tactile Feedback

Iris Jiang
University of Washington

Yuki Ishikawa
University of Tokyo

Jack Lindsay
University of Washington

Blake Hannaford
University of Washington

ABSTRACT

Vibration motors are often used to generate tactile feedback to enhance human-machine interactions and provide information about the environment. We are interested in using these motors to enhance user feedback when wearing below-knee prostheses by providing informational cues via vibrations on the thigh. Our initial designs to hold the motors against the thigh resulted in a weak perception of vibration. We took an engineering approach to improve sensation by modeling the system and designing a new device that maximized skin displacement. Our results show the new suspended design increased skin displacement for both types of vibrational motors.

KEYWORDS: Vibrotactile haptics, skin vibration, mechanical model, optimization, mechanical impedance

1 INTRODUCTION

Skin is a very effective channel for conveying information through the sense of touch. Sensations on the skin can be localized [1], recognized quickly [2-3], and require a low cognitive load to process [4]. Vibrotactile feedback in particular has been commonly used for sensory substitution [5-8], navigation [2, 9], virtual environment interfaces [6, 10], and rehabilitation [10-12]. Placement of a vibrotactile actuator is versatile, so different locations can be stimulated depending on the application.

Vibrational motors used on the skin tend to be small and light weight [13]. The most common types of actuators are linear resonance actuators (LRAs) and eccentric rotating mass motors (ERMs). LRAs operate by oscillating an electric field to vibrate a magnet connected to the case by a spring, and require an AC input. ERMs are DC motors that have an offset mass rotating about the center axis. The non-symmetric rotating mass causes displacement of the motor body at high frequencies to produce vibration.

Lower body amputees suffer from a lack of feedback from their prosthetics and have a high incidence of tripping and falling [14-15]. Providing haptic feedback about the state of the prosthetic leg provides a means to decrease these harmful occurrences [16]. Notifying users early on about a loose fitting socket, which causes pistoning and instability [17], can prompt them to add more socks until the fit is snug. Additionally, we might be able to warn users of immediate dangers which will lead to immediate falls, such as catching the foot or stepping on a slippery surface.

These signals require fast response, and vibrating motors can be actuated in under 20 milliseconds [18]. The compactness and speed of these motors in addition to the skin's ability to sense vibrations make vibration a great method for delivering information from a prosthetic leg to its user.

We have designed a warning system focused on providing feedback at or near the interface between the residual limb and the prosthesis. This provides specificity for the leg and convenience for the user who can easily don the prosthesis along with our device. The entire system has two main components: (1) Sensors and algorithms to detect instability, and (2) Delivery of vibrotactile feedback to the thigh. This paper focuses on (2).

We initially designed a housing for an LRA that held the motor to the thigh via an elastic band. However, due to lower sensation in the thigh compared to other parts of the body [19-20], initial tests resulted in weak stimulation. We think a large contributing factor is due to our block design, which couples the vibrating motor with the damping of the elastic band and skin. Herein, we analyze and simulate the mechanical system in order to design a more efficient holder that maximized the amount of skin displacement. We will also evaluate an ERM designed to produce larger vibrations than the LRA.

Accurately modeling this interface requires understanding of skin mechanics. Skin can be approximately described as a viscoelastic mechanical system [21]. When in contact with a mechanical interface, there is an effective impedance presented by the skin to the mechanical device [22]. Skin's mechanical impedance depends on contact area [23], location on the body [24], frequency [25], and indentation [26]. All of these variables have a complex interaction and affect skin elasticity in a non-linear pattern [27]. We will use the skin model described in Lindsay's [28] paper as he accounts for the same parameters we are interested in.

Mechanical systems like our vibrotactile actuators have a resonant frequency to which they respond most efficiently to vibrations [29]. At this frequency, mechanical impedance is low and little energy is required for the whole system to vibrate at a large amplitude [24]. By placing the actuator in a suspension system tuned to its resonant frequency, we hope to increase the amplitude of vibration. In addition, we have decoupled the vibrating mass from the elastic band in order to more efficiently transfer vibration energy from the actuator to the skin.

Using our mechanical model and numerical optimization, we designed new holders for both LRAs and ERMs that theoretically increased skin displacement. This paper will describe the new design, engineering optimization, and test results for the new and initial holder prototypes.

2 METHODS

2.1 Model

Two basic holders, which we will call the block design, were 3D printed (Dimension bst 768, Stratasys, MN) in Acrylonitrile butadiene styrene (ABS) plastic (Figure 1). The design goal was to hold the vibrational actuators comfortably against the skin without blocking their motion.

A mechanical model of each system was designed using the standard system diagram approach (Figure 2). In our system, the vibrational actuator has a rigid connection to the block holder,

Email: ijiang@uw.edu
Email: ishikawa@robot.t.u-tokyo.ac.jp
Email: jackicl@uw.edu
Email: blake@uw.edu

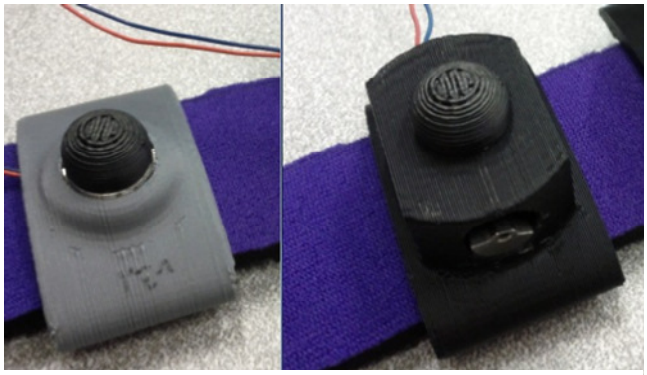

Figure 1: Original block holders mounted on a purple elastic band. (Left) Block LRA holder, (right) Block ERM holder.

which is held in contact with the skin by an elastic band. The models of the actuators were created by direct analysis of the C10-100 LRA and a Pico Vibe 307-002 (Precision Microdrives, London, UK).

The holder is modeled by a single mass mounted with an accelerometer. M_{att} is the mass of the holder in rigid contact with the vibrating motor. M_{acc} is the mass of the accelerometer which is attached to the holder for data collection. This total mass (M_{att} + M_{acc}) is then held by an elastic band with properties K_{ba} and B_{ba} against the skin, which is described by K_s and B_s.

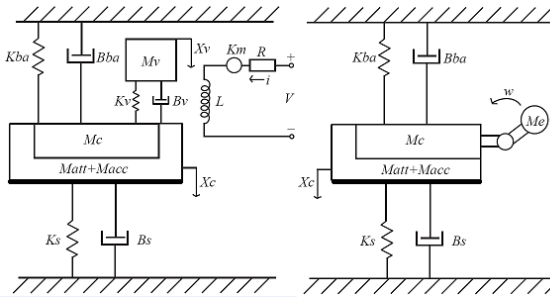

Figure 2: LRA (left) and ERM (right) mechanical models of original housing designs applied to skin. Bold surface denotes *A*

The model for the LRA system can be described by the following equations of motion:

$$Li + iR + K_m(\dot{x}_c - \dot{x}_v) = V \quad (1)$$

$$M_v\ddot{x}_v + B_v(\dot{x}_v - \dot{x}_c) + K_v(x_v - x_c) = -K_m i \quad (2)$$

$$M_t\ddot{x}_c + B_v(\dot{x}_c - \dot{x}_v) + K_v(x_c - x_v) + (B_s - B_{ba})\dot{x}_c + (K_s + K_{ba})x_c = 0 \quad (3)$$

$$M_t = M_c + M_{att} + M_{acc} \quad (4)$$

The model for the ERM system can be described by the following equation of motion:

$$M_t\ddot{x}_c + (B_s + B_h)\dot{x}_c + (K_s + K_h)x_c = M_e r\omega^2 \sin(\omega t) \quad (5)$$

For each device we can transform the equations of motion into the form $\dot{x} = Ax + Bu$. The csim() utility in Scilab [30] was used to simulate the response time of this system to sinusoidal inputs. The input to the LRA (V) had an amplitude of 5V (10V peak-to-peak) and a frequency of 175 Hz. The input to the ERM (ω) was 942 rad/sec. Since we cannot model perception, our best prediction of vibrotactile sensation is to simulate skin displacement (x_s) and measure peak displacement values.

Parameter values (Tables 1-3) were taken from datasheets, measured in the lab, or taken from related literature. Masses were found by weighing the components after disassembly. The elasticity, damping, and motor constant of the LRA and elasticity and damping of the skin were taken from previous work by Lindsay [28]. The band is made from 3mm thick neoprene and its spring and damping properties were calculated by measuring its oscillation frequency and relaxation time constant when loaded with a known mass and allowed to oscillate.

Param	Description	Value	Source
K_s	Skin elast.	600-1200 *N/m*	[28]
B_s	Skin damp.	0.75-2.38 *Nsec/m*	[28]
M_{acc}	Acc. Mass	0.7 *g*	Measured
K_{ba}	Band elast.	16 *N/m*	Measured
B_{ba}	Band damp.	14 *Nsec/m*	Measured

Table 1: Common model parameters

Param	Description	Value	Source
L	Inductance	130μH	Datasheet
R	Resistance	28Ω	Datasheet
M_v	Moving mass	1.4*g*	Measured
M_c	Case mass	0.6*g*	Measured
K_v	LRA elast.	2800 *N/m*	[28]
B_v	LRA damp.	0.0322 *Nsec/m*	[28]
K_m	Motor const.	1	[28]
M_{att}	Holder mass	2.3*g*	Measured

Table 2: LRA model parameters

Param	Description	Value	Source
M_e	Eccentric mass	1.7*g*	Measured
r	Radius of rotation	1.43*mm*	Calculated
M_c	Case mass	1.2*g*	Measured
M_{att}	Holder mass	4.8*g*	Measured

Table 3: ERM model parameters

2.2 New device design

Our original LRA attached to a block holder elicited a very weak sensation when applied to the thigh. Based on our insight that the actuator needed to be decoupled from the strap and body, we designed a new device that suspended the motor in the middle of the holder. This new design (Figure 3) also serves to decrease the mass (M_{att}+M_{acc}) that the motor must vibrate and therefore increase the energy devoted to skin displacement.

Our suspension system used silicone (Permatex, Hartford, CT) that was molded into a six-spoke ring that suspended the moving mass in the center of the holder. The dimensions of each spoke were calculated using Young's modulus (average of 3Mpa) to produce the desired K_h found by our optimization. The molds were printed with a 3D printer, filled with silicone, left to cure over 48 hours, and finally the silicone was removed (Figure 4).

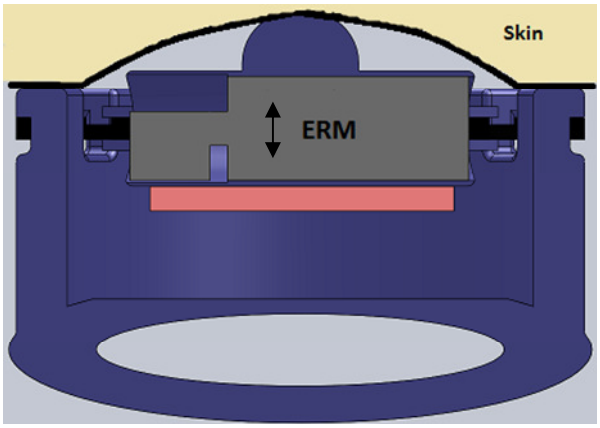

Figure 3: Cross section of Solidworks model of new suspended design. Black represents silicone suspension system that holds the moving mass in the center. Red shows surface measured for displacement and arrow denotes direction of movement.

Figure 4: Image of silicone suspension system for LRA (left) and ERM (right).

In order to optimize K_h, we first created a mechanical model for this new suspension system (Figure 5).

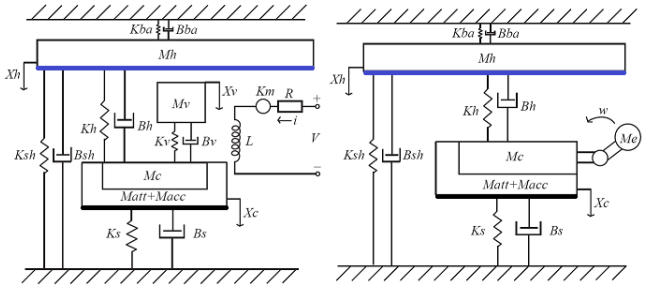

Figure 5: LRA (left) and ERM (right) mechanical models of new suspension housing designs applied to skin. Bold black line denotes *A* and bold blue line denotes A_h

The model for the LRA system can be described by the following equations of motion:

$$Li + iR + K_m(\dot{x}_c - \dot{x}_v) = V \quad (6)$$

$$M_v\ddot{x}_v + B_v(\dot{x}_v - \dot{x}_{c)} + K_v(x_v - x_c) = -K_m i \quad (7)$$

$$M_r\ddot{x}_c + B_v(\dot{x}_c - \dot{x}_v) + K_v(x_c - x_v) + B_s\dot{x}_c + K_s x_c + B_h(\dot{x}_c - \dot{x}_h) + K_h(x_c - x_h) = K_m i \quad (8)$$

$$M_h\ddot{x}_h + B_h(\dot{x}_h - \dot{x}_c) + K_h(x_h - x_c) + (B_{ba}+B_{sh})\dot{x}_h + (K_{ba}+K_{sh})x_h = 0 \quad (9)$$

The model for the ERM system can be described by the following equations of motion:

$$M_r\ddot{x}_c + B_s\dot{x}_c + K_s x_c + B_h(\dot{x}_c - \dot{x}_h) + K_h(x_c - x_h) = M_e r\omega^2 \sin(\omega t) \quad (10)$$

$$M_h\ddot{x}_h + (B_{ba}+B_{sh})\dot{x}_h + (K_{ba}+K_{sh})x_h + B_h(\dot{x}_h - \dot{x}_c) + K_h(x_h - x_c) = 0 \quad (11)$$

2.3 Optimization of suspended design

With the new suspended model, we began to study the effects of each parameter on skin displacement. Initial simulations showed that varying the contact area between the device and the skin (A_h), the mass that holds the motors (M_{att}), and spring constant (K_{ba}) had a large effect on skin displacement x_s.

A brute force numerical search was performed over 6 parameters (K_h, B_h, A_h, A, M_{att}, M_h) to maximize skin displacement (Table 4). The search bounds for K_h and B_h were set at 10^{-3} and 10^3 with exponentially increasing increment values. The search bounds for A_h and A were set at 10^0 and 10^3, also incremented exponentially. The search bound for M_{att} was set at 0.1 and 10.0g and incremented at intervals of 0.1. The search bound for M_h was set at 0.1 and 50.0g and incremented at intervals of 0.1. The mass of the accelerometer (Table 1) attached to the moving mass was accounted for in this optimization.

Param	Description	# Vals	Search Range
K_h	Holder elasticity	133	$10^{-3} - 10^3$ *N/m*
B_h	Holder damping	82	10^{-3}–10^3*Nsec/m*
A_h	Contact area (holder)	46	$10^0 - 10^3$ mm^2
A	Contact area (moving mass)	46	$10^0 - 10^3$ mm^2
M_{att}	Mass attached to motor	100	0-10*g*
M_h	Mass of holder	500	0.1-50*g*

Table 4: Parameter search ranges and number of values within the range that was searched.

After searching through a large range, we refined our search range around initial results.

2.4 Displacement test

A laser sensor (Keyence, NJ; model IL-030) and amplifier (Keyence IL-1000) was used to measure displacement of the moving mass against the skin. We assumed the moving mass stays in contact with the skin as it vibrates, thus we can infer skin displacement. Data from the laser was read with an oscilloscope (Tektronix TDS3032).

Amplification was 1mV per 1µm of displacement. This was verified by shining the laser on a desk and then sliding a washer of .3mm thickness underneath the laser to confirm correct voltage change (300mV). The laser was finally secured in a position above the vibrating device within the measurement rage of 20-45mm.

The four holders were printed using a 3D printer (Figure 1 and 6). Holes were drilled in the back of the suspended designs to allow the laser to measure the movement of the moving mass. A piece of white cardstock paper was hot glued to the surface measured to provide better reflection for the laser. The housings were connected to an elastic band through the loop hole, and the elastic band held the device against the skin on the thigh during the data collection.

The LRAs were driven with a square wave, ±5V at 175 Hz. The ERMs were driven with a DC power supply at 1.5 V.

3 RESULTS

3.1 Initial Simulation

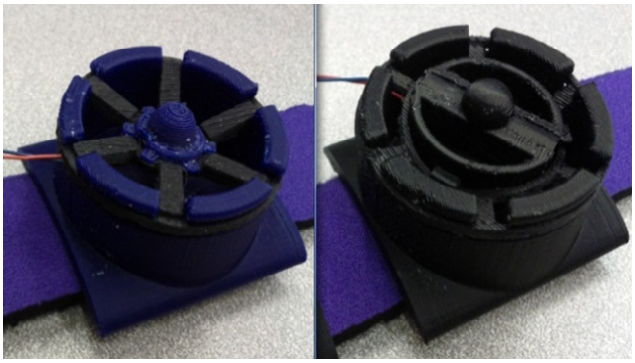

Figure 6: LRA (left) and ERM (right) new suspension designs

We first simulated the models of our original devices. Figure 7 (red lines) shows the simulated skin displacement of the initial block designs. Maximum displacement values are shown in Table 6.

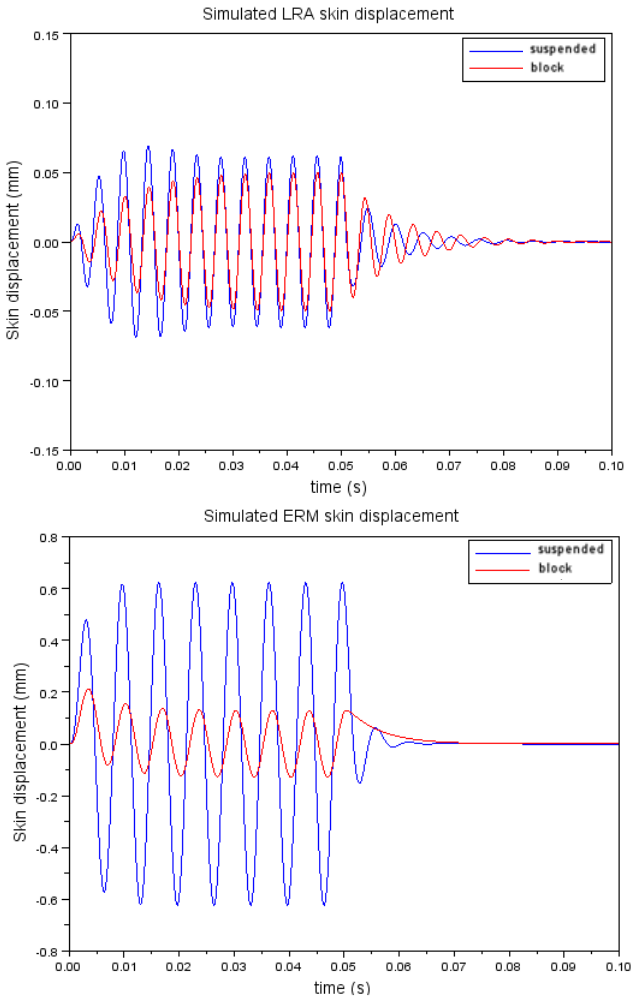

Figure 7: Simulated skin displacement. Top: LRA block vs suspension design, Bottom: ERM block vs suspension. *Note the different scales on the y-axis.

3.2 Optimization for skin displacement

The results of the numerical search for the two new suspension devices yielded parameter values which maximized skin displacement (Table 5). The new devices were then simulated using these optimized parameter values and results are shown by the blue lines in Figure 7. Maximum displacement values are shown in Table 6.

Parameter	Optimal Value (LRA)	Optimal Value (ERM)
K_h	1700 *N/m*	2200 *N/m*
B_h	0.001 *Nsec/m*	0.001 *Nsec/m*
A_h	306 mm^2	306 mm^2
A	314 mm^2	314 mm^2
M_{att}	$0.3g$	$1.2g$
M_h	$10.2g$	$10.9g$

Table 5: Optimal parameter values used in new devices.

3.3 Displacement

Displacement data from the laser sensor was collected with an oscilloscope. Amplitudes (Table 6) were estimated from the oscilloscope readouts and converted to distance at the ratio of 1mV to 1μm. Maximum displacement was taken to be half of the peak-to-peak amplitude to stay consistent with our simulations that describe the motor oscillating about the surface of the skin, which is zero displacement.

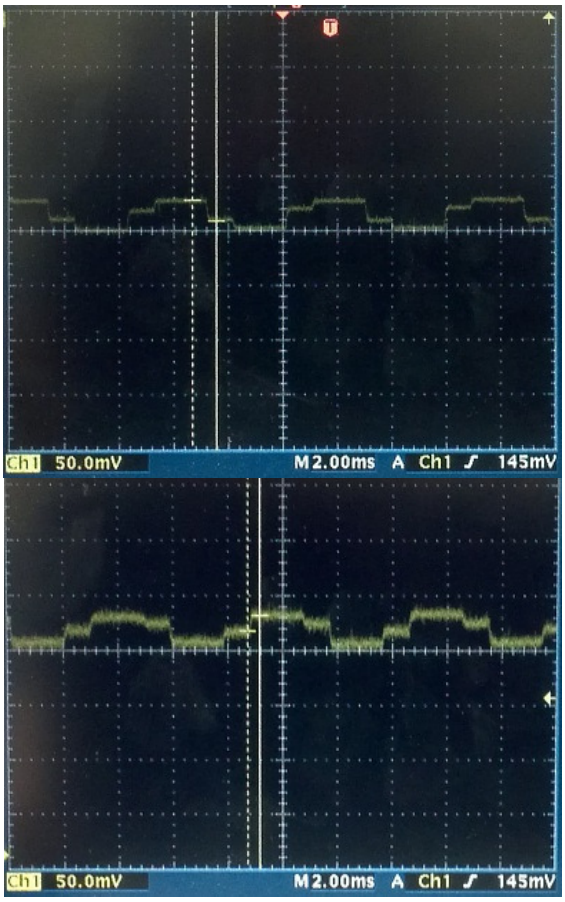

Figure 8: Measured skin displacement for LRA devices. Top: Block design Bottom: Suspension design
* Note the different scales between Figures 8 and 9

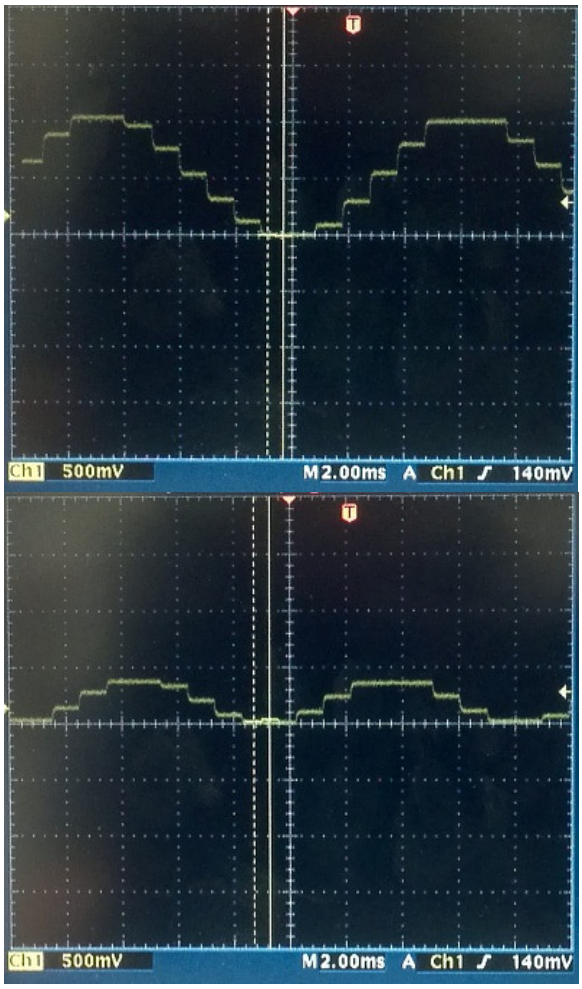

Figure 9: Measured skin displacement for ERM devices. Top: Block design Bottom: Suspension design
* Note the different scales between Figures 8 and 9

	Old design		New design	
	Simulated	**Measured**	**Simulated**	**Measured**
LRA(max)	0.0506	0.015	0.0696	0.018
ERM(max)	0.291	.19	0.892	.5

Table 6: Maximum displacement values (mm)

4 Discussion and Conclusions

We have described simulation, prototyping, and data collection experiments to study vibrotactile holder modifications towards optimization of skin displacement. We studied two actuator types (LRA and ERM) and two mounting systems. Our results focus on skin displacement, which we assume correlates with perception.

Maximum displacement of the suspended LRA increased by a factor of 1.38 in the simulation and by a factor of 1.2 when measured. The simulation of the LRA models and the actual measured values are similar, with the new LRA design only slightly increasing the displacement.

Maximum displacement increased by a factor of 3.07 in the simulation and increased by a factor of 2.63 when measured. The simulation and measured results show similar improvement with the suspended design.

Both types of motors showed some improvement using the suspended design, but the absolute displacement values do not agree. However, this discrepancy can be attributed to the poor resolution of the oscilloscope measurements. More precise measurements could improve agreement between simulation and measured results.

Additionally, there may be inaccuracies in our skin model, which assumes zero displacement when the motor sits on the skin. It is more likely that there is some initial depression, and max displacement should be the peak-to-peak amplitude.

In this work, we focus on skin displacement, but in actuality, human perception of vibration is correlated with more than skin displacement. Future work will test these devices on human subjects in order to determine actual perception instead of just skin displacement. Using our test methods, we hope to be able to quantify the relationship between skin displacement and perception.

Conclusion

This paper demonstrates the ability to increase skin displacement of a vibrotactile actuator by optimizing holder design. Simulations of the new suspended optimized designs showed marked improvement in skin displacement over the old block designs. Data collected with an accelerometer show some agreement between the simulation and experiment of the two LRA designs. However the ERM measurements suggest other factors may be at play. Validation of a more effective holder ultimately lies in testing human subjects for perception as well as skin displacement.

Acknowledgements

The authors wish to thank Professor Hajime Asama and Andy Lewis for their contributions to this project. This work was supported in part by a grant from the NSF Center for Sensorimotor and Neural Engineering.

References

[1] Cholewiak, R.W., J.C. Brill, and A. Schwab, *Vibrotactile localization on the abdomen: Effects of place and space.* Attention, Perception, & Psychophysics, 2004. **66**(6): p. 970-987.

[2] Sergi, F., et al. *Forearm orientation guidance with a vibrotactile feedback bracelet: On the directionality of tactile motor communication*. in *Biomedical Robotics and Biomechatronics, 2008. BioRob 2008. 2nd IEEE RAS & EMBS International Conference on*. 2008: IEEE.

[3] Ammons, R.B., *Effects of knowledge of performance: A survey and tentative theoretical formulation.* The Journal of general psychology, 1956. **54**(2): p. 279-299.

[4] Spirkovska, L., *Summary of tactile user interfaces techniques and systems.* 2004.

[5] Sparks, D.W., et al., *Investigating the MESA (Multipoint Electrotactile Speech Aid): the transmission of segmental features of speech.* The Journal of the Acoustical Society of America, 1978. **63**: p. 246.

[6] Collins, C.C., *Tactile television-mechanical and electrical image projection.* Man-Machine Systems, IEEE Transactions on, 1970. **11**(1): p. 65-71.

[7] Bliss, J.C., et al., *Optical-to-tactile image conversion for the blind.* Man-Machine Systems, IEEE Transactions on, 1970. **11**(1): p. 58-65.

[8] Richardson, B. and M. Symmons, *Vibrotactile devices for the deaf: are they out of touch?* The Annals of otology, rhinology & laryngology. Supplement, 1995. **166**: p. 458.

[9] Piateski, E. and L. Jones. *Vibrotactile pattern recognition on the arm and torso*. in *Eurohaptics Conference, 2005 and Symposium on Haptic Interfaces for Virtual Environment and Teleoperator Systems, 2005. World Haptics 2005. First Joint*. 2005: IEEE.

[10] Holden, M.K., *Virtual environments for motor rehabilitation: review.* Cyberpsychology & behavior, 2005. **8**(3): p. 187-211.

[11] Henderson, A., N. Korner-Bitensky, and M. Levin, *Virtual reality in stroke rehabilitation: a systematic review of its effectiveness for upper limb motor recovery.* Topics in stroke rehabilitation, 2007. **14**(2): p. 52-61.

[12] Piron, L., et al., *Virtual environment training therapy for arm motor rehabilitation.* Presence: Teleoperators & Virtual Environments, 2005. **14**(6): p. 732-740.

[13] Alahakone, A. and S.M.N.A. Senanayake. *Vibrotactile feedback systems: Current trends in rehabilitation, sports and information display*. in *Advanced Intelligent Mechatronics, 2009. AIM 2009. IEEE/ASME International Conference on*. 2009: IEEE.

[14] Miller, W.C., M. Speechley, and B. Deathe, *The prevalence and risk factors of falling and fear of falling among lower extremity amputees* 1.* Archives of physical medicine and rehabilitation, 2001. **82**(8): p. 1031-1037.

[15] Aziz, O. and S. Robinovitch, *An Analysis of the Accuracy of Wearable Sensors for Classifying the Causes of Falls in Humans.* IEEE Trans Neural Syst Rehabil Eng., 2011. **[Epub ahead of print]**.

[16] Fan, R.E., et al. *Pilot testing of a haptic feedback rehabilitation system on a lower-limb amputee*. 2009: IEEE.

[17] Newton, R.L., D. Morgan, and M.H. Schreiber, *Radiological evaluation of prosthetic fit in below-the-knee amputees.* Skeletal radiology, 1988. **17**(4): p. 276-280.

[18] PrecisionMicrodrives. *Website*. 2012.

[19] Bell-Krotoski, J., S. Weinstein, and C. Weinstein, *Testing sensibility, including touch-pressure, two-point discrimination, point localization, and vibration.* Journal of hand therapy: official journal of the American Society of Hand Therapists, 1993. **6**(2): p. 114.

[20] Coren, S., L.M. Ward, and J.T. Enns, *Sensation and perception*. 2003: Wiley.

[21] Agache, P., et al., *Mechanical properties and Young's modulus of human skin in vivo.* Archives of dermatological research, 1980. **269**(3): p. 221-232.

[22] Howe, R. and A. Hajian, *Identification of the mechanical impedance at the human finger tip.* Journal of Biomechanical Engineering, 1997. **119**: p. 109-114.

[23] Verrillo, R.T., *Vibrotactile thresholds for hairy skin.* Journal of Experimental Psychology; Journal of Experimental Psychology, 1966. **72**(1): p. 47.

[24] Lundström, R., *Local vibrations—mechanical impedance of the human hand's glabrous skin.* Journal of biomechanics, 1984. **17**(2): p. 137-144.

[25] Moore, T.J. and J.R. Mundie, *Measurement of specific mechanical impedance of the skin: effects of static force, site of stimulation, area of probe, and presence of a surround.* The Journal of the Acoustical Society of America, 1972. **52**(2B): p. 577-584.

[26] Fritschi, M., et al. *Construction and first evaluation of a newly developed tactile shear force display*. in *Proceedings of the 4th International Conference EuroHaptics 2004*. 2004: Citeseer.

[27] Hendriks, F., et al., *A numerical-experimental method to characterize the non-linear mechanical behaviour of human skin.* Skin research and technology, 2003. **9**(3): p. 274-283.

[28] Lindsay, J., R. Adams, and B. Hannaford, *Improving Tactile Feedback with an Impedance Adapter.* 2012, University of Washington.

[29] Franke, E.K., *Mechanical impedance of the surface of the human body.* Journal of applied physiology, 1951. **3**(10): p. 582-590.

[30] Scilab. *Website*. 2012; Available from: http://www.scilab.org.